Journal of Alloys and Compounds 509 (2011) 5725–5730

Contents lists available at ScienceDirect

Journal of Alloys and Compounds

journal homepage: www.elsevier.com/locate/jallcom

# Synthesis and upconversion luminescence properties of monodisperse $Y_2O_3$:Yb, Ho spherical particles

Mingming Xing[a,*], Wanghe Cao[a], Haiyang Zhong[a], Yinghui Zhang[a], Xixian Luo[a], Yao Fu[a], Wei Feng[a], Tao Pang[a], Xiaofei Yang[b]

[a] Department of Physics, Dalian Maritime University, Dalian 116026, PR China
[b] Jiangsu Province Key Laboratory of Mordern Optical Technology, SooChow University, Suzhou 215006, PR China

ARTICLE INFO

*Article history:*
Received 10 August 2010
Received in revised form 23 February 2011
Accepted 23 February 2011
Available online 3 March 2011

*Keywords:*
Upconversion luminescence
$Y_2O_3$:Yb, Ho
Homogeneous precipitation method

ABSTRACT

Monodispersed spherical $Y_2O_3$:Yb, Ho upconversion luminescence (UCL) particles with sizes of 40–200 nm are prepared using a homogeneous precipitation method. It is found that aging time, varying between 90 and 10 min, has a profound influence on the precursor size, which systematically decreases from 230 nm to 50 nm. The precursor shows poor stability when aging time is 10 min, and the stability of precursor can be improved by increasing the urea concentration. The UCL spectra of $Y_2O_3$:Yb, Ho with different particle sizes are investigated. The results indicate that the integrated emission intensity ratio of green to red ($R_{green/red}$) exhibits a gradual decrease from 2.7 to 0.45 when the particle size decreases from 200 nm to 40 nm, and the possible reasons are evaluated.



## 1. Introduction

There exists a great deal of interest in the trivalent rare-earth ions doped upconversion luminescence (UCL) materials because of their potential application in the fields of solid state laser, laser antiforgery, full color displays, fluorescent biological labels and so on [1–4]. Among the trivalent rare-earth ions, $Ho^{3+}$–$Yb^{3+}$ is a much efficient UCL system [4–9]. However, most of these reported works were concentrated on single crystals and glass materials [7–9], and these materials are less suitable for the applications of antiforgery and fluorescent biological labels as compared with powdered materials. $Y_2O_3$ is a promising host for upconversion powdered phosphor, because it possesses excellent chemical stability and low phonon energy [10] that can suppress the non-radiative multiphonon relaxation and offer a highly efficient UCL. Besides the luminescent efficiency, the application of UCL materials is also related closely to the morphology, size and size distribution of particles. For example, monodisperse spherical fine particles are the primary prerequisite for bioassay and high resolution color display [11,12].

Researchers have developed several techniques to control the size and morphology of UCL particles, such as sol–gel method [13], thermolysis method [14], emulsion liquid membrane method [15] and homogeneous precipitation method [16]. Among above methods, homogeneous precipitation method not only has the advantages such as simple process and low production cost, but also is an effective way to synthesize spherical particles [17,18]. In the present work, we successfully prepared monodisperse spherical $Y_2O_3$:Yb, Ho particles with size in the range of 40–200 nm via a simple homogeneous precipitation method. The effect of aging time, nitrate concentration and urea concentration on the size and stability of precursor particles were systematically investigated. In addition, the size-dependent UCL properties were discussed in detail. The monodisperse spherical upconversion particles are expected to apply in the fields of displays, fluorescent labels, etc.

## 2. Experimental

$Y(NO_3)_3{\cdot}6H_2O$ (99.99%), $Yb(NO_3)_3{\cdot}6H_2O$ (99.99%), $Ho(NO_3)_3{\cdot}6H_2O$ (99.99%) and urea (analytical grade) were used as the raw materials in this work. Typically, the $Y(NO_3)_3$, $Yb(NO_3)_3$ and $Ho(NO_3)_3$ stock solutions were weighed out on the stoichiometry (the doped concentrations of $Yb^{3+}$ and $Ho^{3+}$ were 6 and 1.2 mol%, respectively.) and mixed with deionized water to obtain a 1200 ml mixture aqueous solution A. Additionally, a proper amount of urea was dissolved in deionized water to form a 400 ml urea stock solution B. Solutions A and B were filtered to remove the impurity, respectively. Solution A was heated to 60 °C in a hot water bath, then solution B was added to bring the solution up to 1600 ml, and subsequently heated to 82 °C. The mixture solution was aged for a period when visible bluish tint occurred. The beaker was then placed in a cold-water bath to quench the reaction, and the solution was turned to be white sol. The white sol was aged at room temperature to obtain white precipitates. The resulting precipitates were separated by centrifugation, washed with deionized water and isopropanol, respectively, then dried at 40 °C for 12 h. Dried precipitates were calcined at 800 °C for 1 h to obtain the $Y_2O_3$:Yb, Ho powders. The experimental conditions of different samples are shown in Table 1.

* Corresponding author. Tel.: +86 411 84728586.
*E-mail address:* xingming1112@126.com (M. Xing).

0925-8388/$ – see front matter © 2011 Elsevier B.V. All rights reserved.
doi:10.1016/j.jallcom.2011.02.135

**Table 1**
Experimental conditions for the preparation of different samples and their particle size observed by TEM.

| Sample | [Rare earth nitrate] (M) | [Urea] (M) | Aging time (min) | Calcination temperature (°C) | Particle size (nm) |
|---|---|---|---|---|---|
| Y1–P | 0.01 | 1 | 10 | – | ~50 |
| Y2–P | 0.01 | 6 | 10 | – | ~50 |
| Y2–O | 0.01 | 6 | 10 | 800 | ~40 |
| Y3–P | 0.01 | 1 | 30 | – | ~100 |
| Y3–O | 0.01 | 1 | 30 | 800 | ~80 |
| Y4–P | 0.01 | 1 | 90 | – | ~230 |
| Y4–O | 0.01 | 1 | 90 | 800 | ~200 |
| Y5–P | 0.007 | 1 | 90 | – | ~150 |
| Y6–P | 0.005 | 1 | 90 | – | ~90 |
| Y7–P | 0.003 | 1 | 90 | – | ~40 |

The morphology of the samples was characterized by Tecnai $G^2$ 20 Transmission Electron Microscope (TEM). Fourier transform infrared (FTIR) spectra were obtained with a Nicolet 550 Magna-IR Spectrometer. The energy dispersive X-ray (EDX) spectra of samples were examined by using the Philips XL-30 scanning electric microscope. The Hitachi F-4500 fluorescence spectrophotometer was utilized to measure the UCL spectra of the samples, the emission slit was 1.0 nm, and the excitation source was 980 nm fiber coupled semiconductor refrigeration laser.

## 3. Results and discussion

Fig. 1(a–c) shows the TEM micrographs of the precursor particles obtained through aging for different times. All other experimental conditions, such as the urea concentration, nitrate concentration, are fixed as given in Table 1. It can be seen that all the precursors are well-dispersed spherical particles, and the particle size increases gradually with the prolonging of aging time. For aging time of 10, 30 and 90 min, the observed particle sizes are about 50, 100 and 230 nm, respectively.

According to the literature data, the stable precursor particles prepared by homogeneous precipitation method should show a fully perfect morphology under a high energy electron beam of TEM [19]. However in this work, it is noteworthy that during the TEM observing process the particles aged for 10 min present some little holes (Fig. 1(a)), while the particles aged for 30 (Fig. 1(b)) and 90 min (Fig. 1(c)) have little change, indicating that the precursor particles prepared by a short aging time are not stable. This phenomenon can be ascribed to the special aggregating growth mechanism [20]. In the aggregation mode, the nuclei grow by molecular addition to form small primary particles in solution firstly. After that, these primary particles will aggregate with each other to yield larger particles, and this process is facilitated by Brownian motion. With the prolonging of aging time the newly gen-

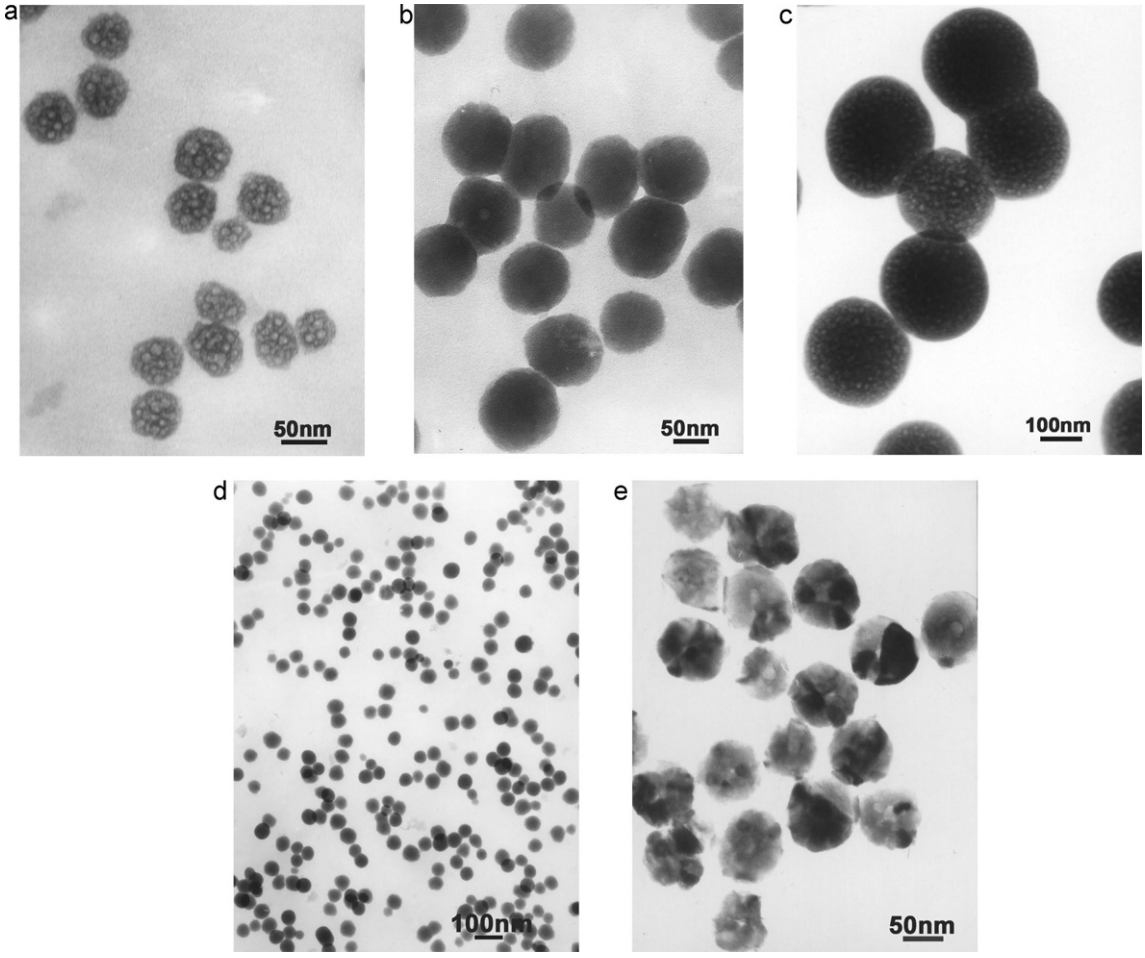


**Fig. 1.** TEM images of different samples: (a) Y1–P, (b) Y3–P, (c) Y4–P, (d) Y2–P and (e) Y3–O.

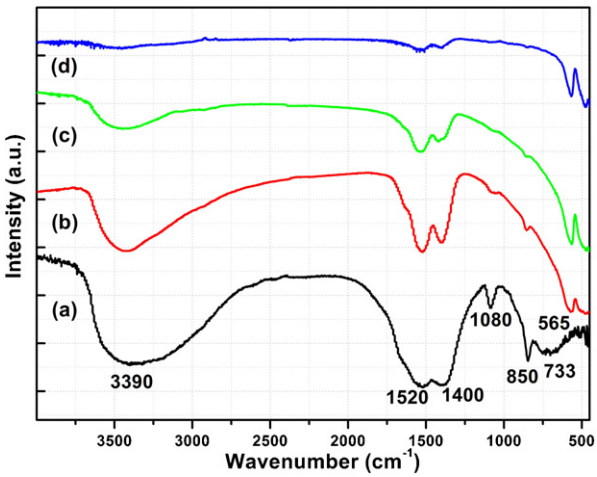


**Fig. 2.** FTIR spectra of different samples: (a) precursor, (b) Y2–O, (c) Y3–O and (d) Y4–O.

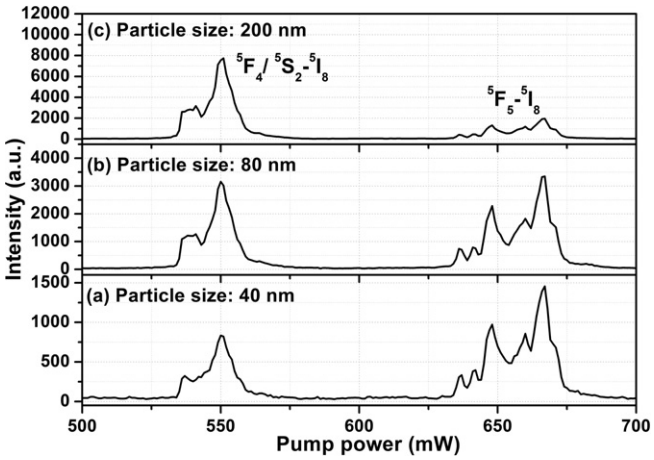


**Fig. 3.** UCL spectra of different samples: (a) Y2–O, (b) Y3–O and (c) Y4–O.

erated nuclei or primary particles will attach to the surface of the larger agglomeration, resulting in the further growth of particles. However, as the aging time shortens up to 10 min, the aggregation of the primary particles is not sufficient, thus we observed the unstable particles in Fig. 1(a).

The stability of the precursor particles can be improved by increasing the urea concentration. For example, when the urea concentration increases up to 6 M, keeping other experimental conditions the same, the particles aged for 10 min (Fig. 1(d)) retain a favorable morphology, and do not observe the changes like in Fig. 1(a) under a high energy electron beam of TEM. This variation can be explained as follows: the higher the urea concentration, the greater the amount of $CO_3^{2-}$ and $OH^-$ hydrolyzed by urea and the larger supersaturation in solution will be. As a result, the nucleation density is increased and the aggregating of the primary particles is accelerated. Therefore, the stability of precursor particles is improved obviously.

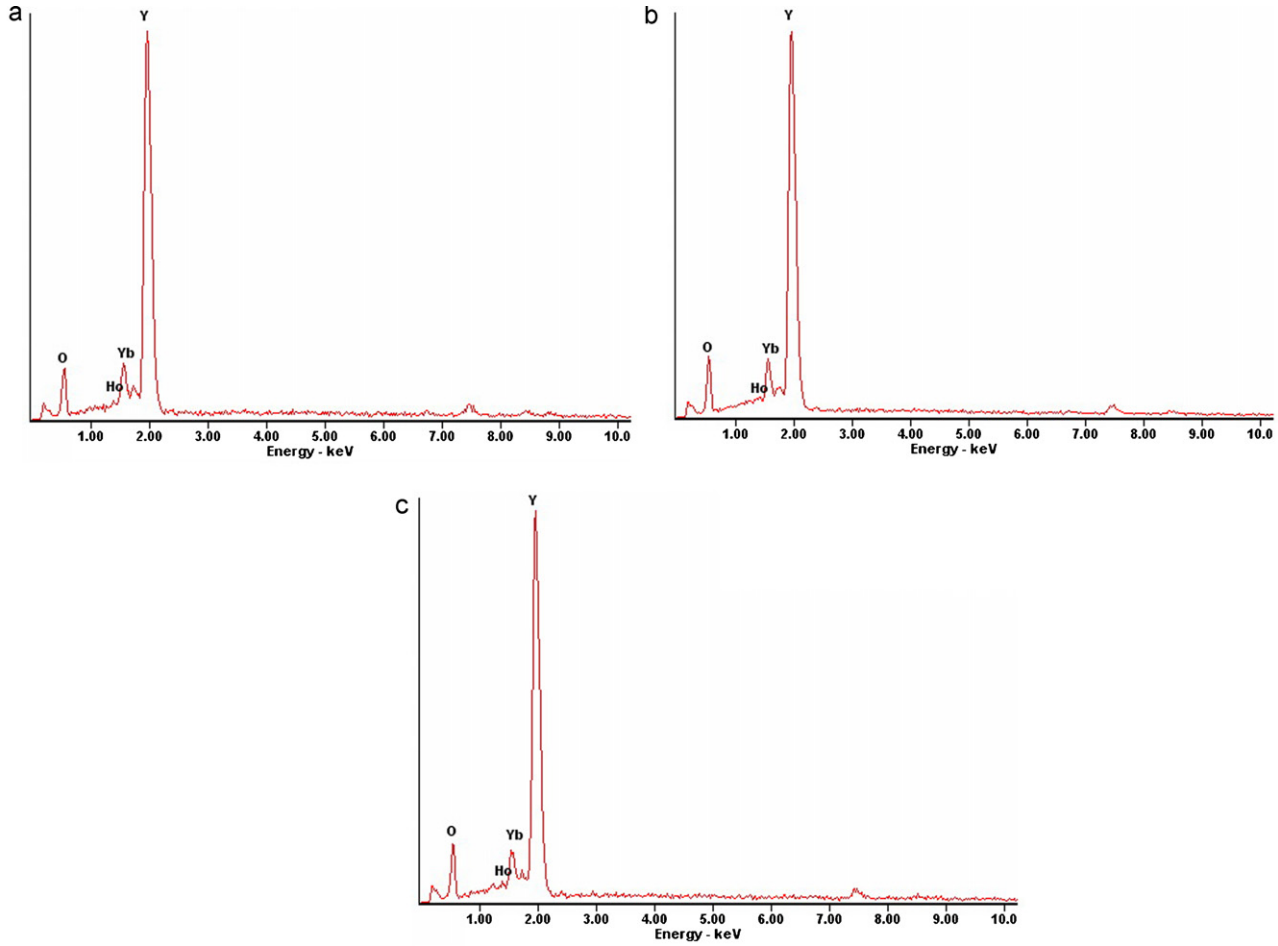


**Fig. 4.** EDX spectra of different samples: (a) Y2–O, (b) Y3–O and (c) Y4–O.

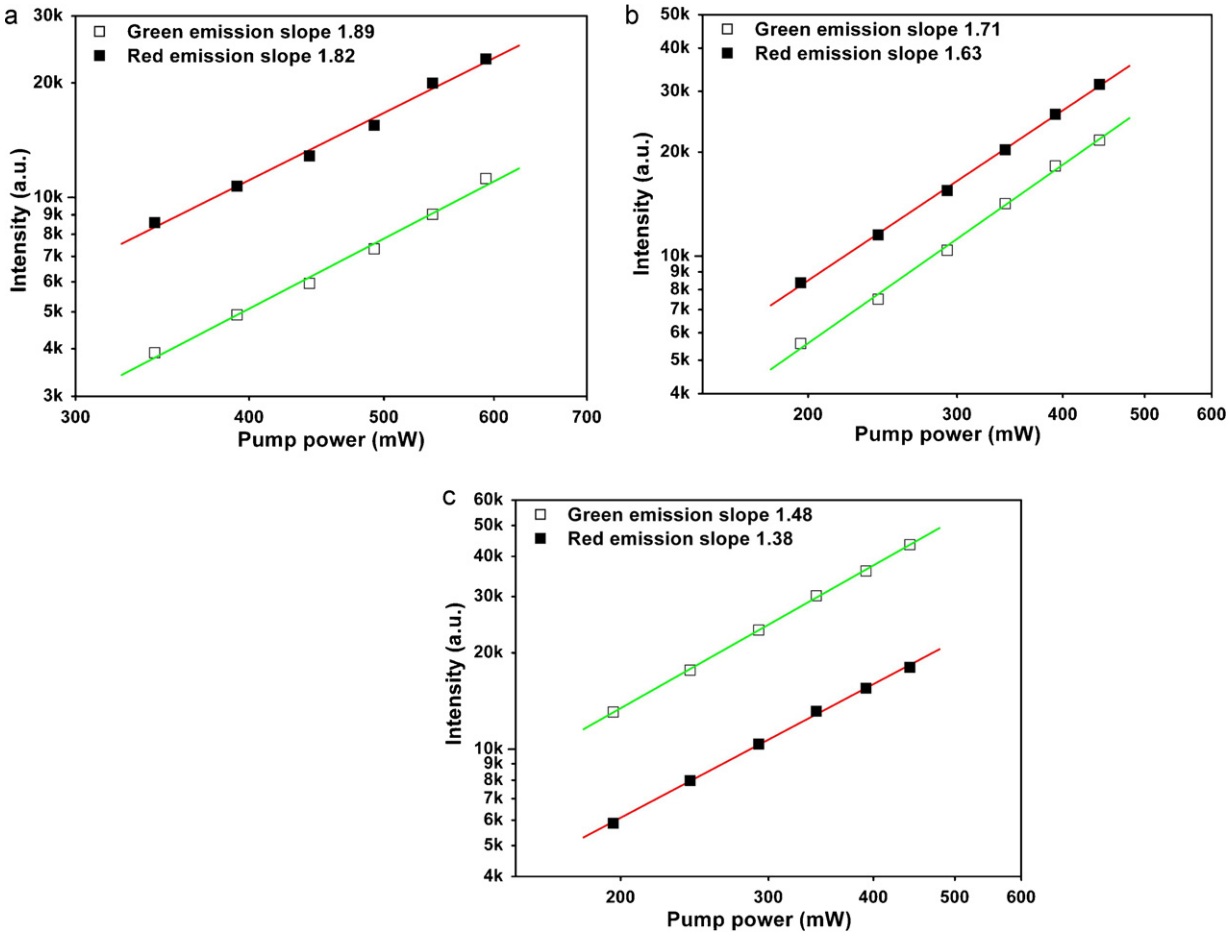


**Fig. 5.** Plot (ln–ln) of UCL intensity versus excitation power in different samples: (a) Y2–O, (b) Y3–O and (c) Y4–O.

On the other hand, the nitrate concentration has a profound impact on the precursor particle size. In the case of urea concentration and aging time fixed at 1 M and 90 min, respectively, as the nitrate concentration increases from 0.003 M to 0.01 M, the corresponding particle size increases from about 40 nm to about 230 nm. The reason for this is that the initial number of nuclei dose not vary with the nitrate concentration, but rather that as the cation concentration increases, the size of the fixed number of particles increases [21].

As noted earlier, the precipitated precursor particles can be converted to crystalline $Y_2O_3$ above 570 °C [12]. It is very important to understand the changes of morphology during the calcination process, since the application of $Y_2O_3$:Yb, Ho particles is very dependent on their shape. Fig. 1 compares the morphology before (b) and after (e) calcinations performed at 800 °C for 1 h. It can be seen that the particle size of calcined sample is reduced by 15–20% as compared with that of precursors. However, particle shape does not change significantly, and it still maintains the shape of the original spherical. This is very beneficial to display application, for spherical phosphor is required for high brightness and high resolution of displays [11].

Fig. 2 shows the FTIR spectra of the precursor and calcined samples, respectively. For all the precursors, the FTIR spectra are identical: the broad absorption band around 3390 $cm^{-1}$ can be assigned to O-H stretching vibration; the bands around 1520 and 1400 $cm^{-1}$ result from C–O asymmetrical stretching vibration; the peak that appears at 1080 $cm^{-1}$ can be assigned to C–O symmetric stretching vibration; the peak at 850 $cm^{-1}$ corresponds to C–O deformation vibrations; the weak peak at 733 $cm^{-1}$ is due to O–H deformation vibration [22]. After calcining at 800 °C for 1 h, the peaks at 1080, 850 and 733 $cm^{-1}$ disappear, and the sharp peak at 565 $cm^{-1}$ associated with the vibration of Y–O is observed, indicating the formation of $Y_2O_3$ [23]. Moreover, as the particle size decreases to nanometer range, due to the high surface-to-volume ratio, large amount of $H_2O$ and $CO_2$ in atmosphere is absorbed on the surface of particles to form $CO_3^{2-}$ and $OH^-$. Thus the bands around 3390, 1520 and 1400 $cm^{-1}$ in calcined powder gradually strengthen along with the decrease of particle size.

Fig. 3 shows the UCL spectra of Y2–O, Y3–O and Y4–O samples under the 980 nm laser excitation. All the UCL spectra consist of two emission bands: (1) the green emission band between 530 and 570 nm with the strongest peak at 550 nm can be attributed to the $^5F_4$, $^5S_2 \rightarrow {}^5I_8$ transition of $Ho^{3+}$ ion; (2) the red emission band between 630 and 675 nm with the strongest peak at 667 nm correspond to the $^5F_5 \rightarrow {}^5I_8$ transition of $Ho^{3+}$ ion. For all the $Y_2O_3$:Yb, Ho samples, the locations of these two emission bands are identical, suggesting that the particle size dose not affect the crystal fields surrounding the $Yb^{3+}$ and $Ho^{3+}$ ions. It is distinctly observed that the integrated emission intensity ratio of the green to the red ($R_{green/red}$) decreases remarkably with decreasing particle size (the $R_{green/red}$ values of Y4–O, Y3–O and Y2–O samples are 2.7, 0.68 and 0.45, respectively). This phenomenon could originate from the different dopant concentrations in samples because the experimental conditions of the samples are different. However, according to the results of EDX, as shown in Fig. 4, the concentrations of dopant in these three samples are nearly identical, thus we rule it out. Based on the above results, it is suggested that the emission light color of $Y_2O_3$:Yb, Ho could be controlled by selecting different particle

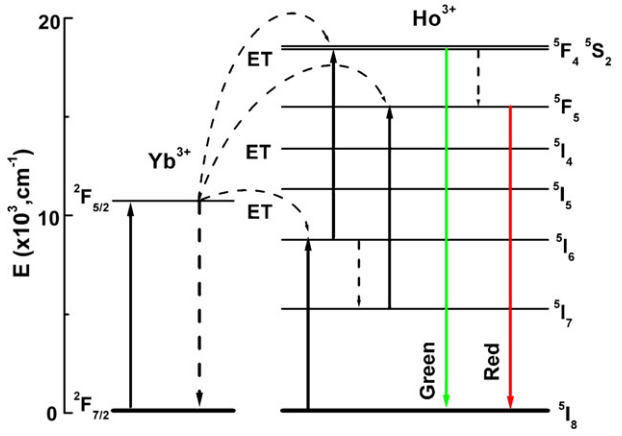


**Fig. 6.** Schematic diagram of the energy levels of $Ho^{3+}$ and $Yb^{3+}$ ions and the upconversion mechanism.

sizes.To explore the reason for the variation of $R_{green/red}$, we should analyze the UCL mechanisms firstly. It is well known that the UCL intensity ($I_{UCL}$) is proportional to some power $n$ of the excitation power ($I_P$) in the upconversion process:

$$I_{UCL} \propto I_P^n$$

where $n$ is the number of absorbed photons required to populate the emission states. Apparently, for all the $Y_2O_3$:Yb, Ho samples the green and red emissions are originated from two-photon process, as shown in Fig. 5.The energy level diagrams of $Yb^{3+}$ and $Ho^{3+}$ together with possible upconversion mechanisms for the green and red emission are presented in Fig. 6. For the green emission, the $Yb^{3+}$ ion is firstly excited from the ground state $^2F_{7/2}$ to the $^2F_{5/2}$ state via absorbing a 980 nm photon and then transfer its energy to the nearby $Ho^{3+}$ ion in the ground state $^5I_8$ by energy transfer (ET) process, thus exciting it to the $^5I_6$ excited state with excess energy (approximately 1200 $cm^{-1}$) transferred to the host lattice. After the first-step excitation, the $Ho^{3+}$ ion of $^5I_6$ state is excited to $^5S_2$ and $^5F_4$ states via another ET or excited state absorption (ESA) process and the energy excess of 600 $cm^{-1}$ is again dissipated by vibration of the host lattice. From $^5S_2$ and $^5F_4$ excited states, the $Ho^{3+}$ ions decay radiatively to the $^5I_8$ ground state generating the green emission. Moreover, it is reported that the $Ho^{3+}$ ion in $^5I_6$ level can also nonradiatively relax to the $^5I_7$ state with the participation of phonons, subsequent ET from $Yb^{3+}$ ion or ESA process are responsible for populating the red emission level $^5F_5$ [9] via the $^5I_7 \rightarrow {}^5F_5$ transition. According to the energy-gap law:

$$p = \frac{\Delta E}{\hbar\omega}$$

where $\Delta E$ is the electronic energy gap, $\hbar\omega$ is maximum phonon energy of the host lattice, the multiphonon relaxation is dominant for $p \leq 5$ [24].

However, in the present work, the calculated $p$ value between $^5I_6$ and $^5I_7$ levels in Y4–O sample is about 5.4 according to the maximum phonon energy of 597 $cm^{-1}$ in $Y_2O_3$ matrix and the energy gap of 3220 $cm^{-1}$ between these two levels. Therefore, the population of red emission level $^5F_5$ in Y4–O sample is mainly originated from the nonradiative relaxation of $^5S_2 \rightarrow {}^5F_5$ due to the relatively ineffective nonradiative relaxation of $^5I_6 \rightarrow {}^5I_7$. While in the case of Y2–O and Y3–O samples, because the high energy vibration modes, such as $CO_3^{2-}$ and $OH^-$, are involved (shown in Fig. 2), the $p$ value between $^5I_6$ and $^5I_7$ levels decreases dramatically to ~1. So the nonradiative relaxation rate of $^5I_6 \rightarrow {}^5I_7$ increases remarkably, which leads to the decreasing of green emissions and the increasing of red emissions in the two samples [25]. This can be further demonstrated by the slope values of the ln–ln plot of the green emission intensity as a function of excitation power. Based on the reports by Pollnau et al. [26] and Song et al. [27,28], for the relation between $I_{UCL}$ and $I_p^n$ ($I_{UCL} \propto I_P{}^n$), where $n = 2$, it indicates the linear decay of the intermediate excited level is dominant; while $n = 1$, it means the upconversion process of the intermediate excited level is dominant.

For $Y_2O_3$:Yb, Ho, the intermediate excited level for green emission is $^5I_6$, and the corresponded $n$ value for the Y4–O sample is 1.48 (shown in Fig. 5(c)). It is suggested that the upconversion process is the dominant depletion mechanism of $^5I_6$ level. While in the Y3–O and Y2–O samples, the $n$ values are increased to 1.71 and 1.89, respectively, showing that the linear decay becomes the dominant depletion mechanism of $^5I_6$ level, Therefore, the green emissions of Y2–O and Y3–O samples are weaker than that of Y4–O sample.

## 4. Conclusions

Monodisperse spherical $Y_2O_3$:Yb, Ho upconversion particles with size in the range of 40–200 nm are successfully prepared using a simple homogeneous precipitation method. The effects of aging time, nitrate concentration and urea concentration on the particle size and stability of precursor particles are studied in detail. The results indicated that the particle size increased with the increase of nitrate concentration, and decreased with the shortening of aging time. Moreover, as the aging time is shortened to 10 min, the precursor is not stable. The stability can be improved by increasing the urea content. Under the excitation of 980 nm, the relative intensities of green to red emissions decrease with decreasing the particle size, which can be attributed to the high energy vibration groups such as $CO_3^{2-}$ and $OH^-$ absorbed on the surface of particles.

## Acknowledgements

The authors thank to the financial support by the National Natural Science Foundation of China (60979003 and 20977012), New Century Educational Talents Plan of Chinese Education Ministry, China (NCET-10-0171), the Scientific Research Projects of Education Department of Liaoning Province (L2010057), the Natural Science Foundation of Liaoning Province (20092146), the National High-teach Research & Development Program (863 Program) (2008AA06Z317), the Program for International S&T Cooperation Projects of the Ministry of Science and Technology of China (2010DFA61470) and the Fundamental Research Funds for the Central Universities, China (2009QN123 and 2009JC22).

## References

[1] F. Wang, X.G. Liu, J. Am. Chem. Soc. 130 (2008) 5642–5643.
[2] H. Eilers, J. Alloys Compd. 474 (2009) 569–572.
[3] E. Garskaite, M. Lindgren, M.A. Einarsrud, T. Grande, J. Eur. Ceram. Soc. 30 (2010) 1707–1715.
[4] X.X. Luo, W.H. Cao, Mater. Lett. 61 (2007) 3696–3700.
[5] R. Lisiecki, G. Dominiak-Dzik, W. Ryba-Romanowski, T. Łukasiewicz, J. Appl. Phys. 96 (2004) 6323–6330.
[6] L.Q. An, J. Zhang, M. Liu, S.W. Wang, J. Lumin. 122–123 (2007) 125–127.
[7] A.S. Gouveia-Neto, E.B. da Costa, L.A. Bueno, S.J.L. Ribeiro, J. Lumin. 110 (2004) 79–84.
[8] F. Lahoz, I.R. Martín, A. Briones, J. Appl. Phys. 95 (2004) 2957–2962.
[9] W. Ryba-Romanowski, S. Golab, G. Dominiak-Dzik, P. Solarz, Appl. Phys. Lett. 79 (2001) 3026–3028.
[10] Y.F. Bai, K. Yang, Y.X. Wang, X.R. Zhang, Y.L. Song, Opt. Commun. 281 (2008) 2930–2932.
[11] Y.C. Kang, S.B. Park, Mater. Res. Bull. 35 (2000) 1143–1151.
[12] X.X. Luo, W.H. Cao, M.M. Xing, J. Mater. Res. 24 (2009) 1756–1760.
[13] D. Solís, T. López-Luke, E. De la Rosa, P. Salas, C. Angeles-Chavez, J. Lumin. 129 (2009) 449–455.
[14] O. Ehlert, R. Thomann, M. Darbandi, T. Nann, Nano Lett. 2 (2008) 120–124.
[15] T. Hirai, T. Orikoshi, I. Komasawa, Chem. Mater. 14 (2002) 3576–3583.
[16] Y.H. Li, G.Y. Hong, Y.M. Zhang, Y.N. Yu, J. Alloys Compd. 456 (2008) 247–250.
[17] I.Y. Park, D. Kim, J. Lee, S.H. Lee, K.J. Kim, Mater. Chem. Phys. 106 (2007) 149–157.

[18] A.I.Y. Happy, F.Y.C. Tok, R. Boey, S.H. Huebner, J. Ng, J. Electroceram. 17 (2006) 75–78.
[19] S. Sohn, Y. Kwon, Y. Kim, D. Kim, Powder Technol. 142 (2004) 136–153.
[20] M.M. Xing, W.H. Cao, T. Pang, X.Q. Ling, Solid State Commun. 149 (2009) 911–914.
[21] D. Sordelet, M. Akinc, J. Colloid Interface Sci. 122 (1988) 47–59.
[22] M.I. Martinez-Rubio, T.G. Ireland, G.R. Fern, J. Silver, M.J. Snowden, Langmuir 17 (2001) 7145–7149.
[23] M.I. Martinez-Rubio, T.G. Ireland, J. Silver, G. Fern, C. Gibbons, A. Vecht, Electrochem. Solid-State Lett. 3 (2000) 446–449.
[24] Q. Lü, F.Y. Guo, L. Sun, A.H. Li, L.C. Zhao, J. Phys. Chem. C 112 (2008) 2836–2844.
[25] G. De, W.P. Qin, J.S. Zhang, J.S. Zhang, Y. Wang, C.Y. Cao, Y. Cui, J. Lumin. 119–120 (2006) 258–263.
[26] M. Pollnau, D.R. Gamelin, S.R. Lüthi, H.U. Güdel, Phys. Rev. B 61 (2000) 3337–3346.
[27] Y.Q. Lei, H.W. Song, L.M. Yang, L.X. Yu, Z. Liu, G.H. Pan, X. Bai, L.B. Fan, J. Chem. Phys. 123 (2005) 174710-1–174710-5.
[28] X. Bai, H.W. Song, G.H. Pan, Y.Q. Lei, T. Wang, X.G. Ren, S.Z. Lu, B. Dong, Q.L. Dai, L.B. Fan, J. Phys. Chem. C 111 (2007) 13611–13617.